Matter and Radiation at Extremes | RESEARCH ARTICLE | scitation.org/journal/mre

Unified first-principles equations of state of deuterium-tritium mixtures in the global inertial confinement fusion region

Cite as: Matter Radiat. Extremes 5, 055401 (2020); doi: 10.1063/5.0008231
Submitted: 19 March 2020 • Accepted: 16 August 2020 •
Published Online: 4 September 2020

Dongdong Kang, Yong Hou, Qiyu Zeng, and Jiayu Dai[a)]

AFFILIATIONS

Department of Physics, National University of Defense Technology, Changsha, Hunan 410073, People's Republic of China

Note: This paper is part of the Special Issue on Atomic and Molecular Physics for Controlled Fusion and Astrophysics.
[a)]**Author to whom correspondence should be addressed:** jydai@nudt.edu.cn

ABSTRACT

Accurate knowledge of the equation of state (EOS) of deuterium–tritium (DT) mixtures is critically important for inertial confinement fusion (ICF). Although the study of EOS is an old topic, there is a longstanding lack of global accurate EOS data for DT within a unified theoretical framework. DT fuel goes through very wide ranges of density and temperature from a cold condensed state to a hot dense plasma where ions are in a moderately or even strongly coupled state and electrons are in a partially or strongly degenerate state. The biggest challenge faced when using first-principles methods for obtaining accurate EOS data for DT fuel is the treatment of electron–ion interactions and the extremely high computational cost at high temperatures. In the present work, we perform extensive state-of-the-art *ab initio* quantum Langevin molecular dynamics simulations to obtain EOS data for DT mixtures at densities from 0.1 g/cm^3 to 2000 g/cm^3 and temperatures from 500 K to 2000 eV, which are relevant to ICF processes. Comparisons with average-atom molecular dynamics and orbital-free molecular dynamics simulations show that the ionic strong-coupling effect is important for determining the whole-range EOS. This work can supply accurate EOS data for DT mixtures within a unified *ab initio* framework, as well as providing a benchmark for various semiclassical methods.

I. INTRODUCTION

Inertial confinement fusion (ICF) is one of the most promising approaches to achieving an unlimited supply of clean energy. In conventional central ignition designs, cryogenic deuterium–tritium (DT) fuel is compressed to a state of high density and high temperature by an imploding ablator driven by strong sources such as intense laser pulses, x-rays generated by laser ablation, and Z-pinches.[1,2] In the process of ICF, the imploding DT fuel goes from a cold condensed state to one of warm dense matter, finally reaching the hot dense plasma regime, where the density covers a wide range from 0.1 g/cm^3 to 1000 g/cm^3 and the temperature varies from several hundred kelvin to a few thousand electronvolts.[3] Accurate knowledge of the thermodynamic properties of DT fuel such as its equation of state (EOS) and its transport coefficient in these wide density and temperature ranges is essential for ICF designs using hydrodynamic simulations.[4–13]

To obtain an accurate EOS of DT mixtures, much effort has been devoted to measuring the Hugoniot and related properties of hydrogen and deuterium under shock compressions driven by gas guns,[14] converging shocks,[15] high-power lasers,[16–18] and magnetically driven fliers.[19,20] However, owing to the complex nature of condensed hydrogen and the challenges faced in the development of suitable diagnostic techniques, there is still a scarcity of experimental data. To date, the pressures reached in the laboratory are limited to several megabars, and the accuracy of shock-compression data is not yet sufficient to establish the reliability of various theoretical models. Consequently, theoretical calculations have become the most important approach to obtaining EOS data over the wide ranges of density and temperature relevant to ICF.[12]

A number of theoretical methods have been developed for calculating the EOS of matter under extreme conditions. EOS data for hydrogen and its isotopes generated by chemical models[21–24] and the SESAME EOS tables[25,26] are widely used in radiation hydrodynamic simulations because these models are computationally efficient. To accurately describe the electronic structure of hot dense plasmas, the average atom (AA) model[27,28] was developed under the assumption of a single-particle spherically symmetric ionic potential. In this

model, a pseudo-atom with an average fractional occupation number for electron orbitals is used to approximately describe the ions in the plasma environment. It should be noted that at high densities, ion–ion interactions could break the spherical symmetry of the ionic potential, and ionic correlation effects must therefore be taken into account. A method that combines the AA model and molecular dynamics simulations (AAMD)[29] has been proposed to treat ionic correlation effects at the level of pair correlations for calculating EOS data for hot dense plasmas. Although these methods have been extensively applied to the high-energy-density plasma regime, they cannot provide a satisfactory description of the strong-coupling state of DT fuel that exists in ICF processes.[30]

At present, two *ab initio* approaches, namely, density functional theory[31–33] (DFT)-based quantum molecular dynamics (QMD)[34–36] and quantum Monte Carlo (QMC) methods,[37–40] are most widely used to calculate the EOS of materials at high densities and temperatures. One of the most promising QMC methods is path-integral Monte Carlo (PIMC),[37,38] which treats ions and electrons quantum-mechanically on the same footing. Another QMC algorithm is coupled electron–ion Monte Carlo (CEIMC),[39,40] which uses the conventional QMC method to obtain the potential energy surface directly. Although both of these have been employed to investigate the thermodynamic properties of hydrogen and its isotopes, the CEIMC predictions disagree with the experimental principal Hugoniot of deuterium,[41] whereas PIMC becomes computationally prohibitive at low temperatures. On the other hand, within the Kohn–Sham–Mermin DFT framework, the ionic strong-coupling effect, which is significant in the high-density region of the DT phase diagram, can be included naturally in QMD, and the key approximation in principle is the exchange-correlation functional. To overcome the prohibitive computational cost of QMD at extremely high temperatures, orbital-free molecular dynamics (OFMD),[42–44] which constructs the approximate noninteracting free energy functional without the assistance of single-electron wavefunctions, and an extended QMD with a plane-wave approximation at high energy have been proposed.[45] Although OFMD is highly efficient, it is inaccurate at low temperatures because it lacks electron orbital information. Some EOS data for hydrogen and deuterium have been obtained by combining the two methods, using QMD at low temperature and a semiclassical method such as OFMD at high temperatures.[6] In this case, the location of the boundary and the transition between the two methods is an essential but challenging task. The quantum Langevin molecular dynamics (QLMD) method was developed for a unified description of matter over a wide range from the cold condensed state to the ideal plasma gas.[46] It not only considers the electron–ion collision effects at high temperatures, which is usually neglected in QMD simulations, but also has a lower computational cost than conventional QMD.[47] QLMD has been successfully applied to calculate the wide-range EOS of hydrogen, hydrogen–helium mixtures, and iron.[48–52]

In this work, we perform extensive simulations to calculate the pressure and internal energy of DT mixtures over wide ranges of density and temperature using *ab initio* QLMD simulations. In contrast to EOS tables obtained by combining various theoretical methods each of which is suitable for different density and temperature ranges, the EOS data presented in this work, which can be used for hydrodynamic simulations of ICF implosions, are obtained for the first time within a unified *ab initio* framework. We also compare the EOS data obtained from QLMD simulations with those from AAMD and OFMD simulations to assess the accuracy of these data and the regions of validity of these methods.

II. COMPUTATIONAL METHOD

A. Quantum Langevin molecular dynamics

In this section, we briefly introduce the QLMD simulation method. In conventional QMD simulations, ions move on the smooth potential surface obtained from Kohn–Sham DFT (KSDFT) calculations of electronic structure within the framework of the Born–Oppenheimer approximation. The physical quantities are averaged over all the configurations along the MD trajectories after a thermalization process. QMD has been extensively applied in a variety of fields from cold condensed matter to warm dense matter. We should note that when matter is in a warm or even a hot dense state, a large number of electrons are excited or ionized. These nearly free electrons form a sea of electrons in warm or hot dense matter, and there are frequent elastic or inelastic electron–ion collisions. There is an analogy between ions in warm or hot dense matter and heavy particles in Brownian motion. In the warm or hot dense regime, ions move in the electron sea as heavy Brownian particles, and electron–ion collisions occur frequently. The effects of these collisions, which are not included in conventional adiabatic QMD simulations, play important roles in determining the structures and thermodynamic properties of warm dense matter. We introduce such electron–ion collision-induced friction (EI-CIF) into the ion dynamics within an adiabatic framework, and we describe the ion motion using the Langevin equation, which takes the form

$$M_I\ddot{\mathbf{R}}_I = \mathbf{F} - \gamma M_I\dot{\mathbf{R}}_I + \mathbf{N}_I, \tag{1}$$

where M_I is the ion mass, $\mathbf{R}_I$ is the ion position, $\mathbf{F}$ is the force calculated from DFT, γ is the friction coefficient, and $\mathbf{N}_I$ is a Gaussian random force.

As a key parameter, the friction coefficient γ plays a central role in QLMD. There are three contributions to γ: $\gamma = \gamma_B + \gamma_f + \gamma_a$. The most important of these, γ_B, represents electron–ion collisions and is derived according to the assumptions of the Rayleigh model,[53]

$$\gamma_B = 2\pi\frac{m_e}{M_I}Z^*\left(\frac{4\pi n_i}{3}\right)^{1/3}\sqrt{\frac{k_BT}{m_e}}, \tag{2}$$

where m_e is the electron mass, n_i is the ion number density, and Z^* is the average degree of ionization, which is obtained by another approach such as the average atom model. The second contribution, γ_f, arises from force errors, i.e., it is the difference between the force obtained with insufficient convergence and that obtained with sufficient convergence in otherwise identical self-consistent-field calculations.[47] The Gaussian distribution of the force errors makes it possible to accelerate the QMD simulation with the Langevin equation. The third contribution, γ_a, is generally used as a conventional Langevin thermostat parameter to maintain a constant temperature. In the warm or hot dense regime, in particular at high temperatures, the electron–ion friction coefficient γ_B makes the dominant contribution to ion motion, and thus γ_f and γ_a can be neglected at relatively high temperatures.

It should be noted that the friction coefficient in Eq. (2) depends on an ion charge Z^* that is determined by an average atom model. This introduces a decidedly non-*ab initio* element to QLMD simulations. In fact, the DT mixture is fully ionized in most of the regime shown in Fig. 1 below. Even if it is only partially ionized, the error introduced in Z^* can be neglected because the friction coefficient is assumed to be in an appropriate range such that the ion–electron collisions and the dynamical behavior are described correctly.[46]

The friction coefficient and the Gaussian random force are connected by the fluctuation–dissipation theorem

$$\langle \mathbf{N}_I(0)\mathbf{N}_I(t)\rangle = 6\gamma M_I k_B T\, dt, \tag{3}$$

where dt is the molecular dynamics time step and the random forces are generated as $\langle \mathbf{N}_I^2\rangle = 6\gamma M_I k_B T/dt$.

We use the Verlet algorithm to integrate the Langevin equation (1),

$$\mathbf{R}_I(t+dt) = \mathbf{R}_I(t) + \frac{1-\frac{1}{2}\gamma_T\, dt}{1+\frac{1}{2}\gamma_T\, dt}[\mathbf{R}_I(t)-\mathbf{R}_I(t-dt)] + \frac{dt^2}{M_I(1+\frac{1}{2}\gamma_T\, dt)}[\mathbf{F}(t)+\mathbf{N}_I(t)], \tag{4}$$

and the ion velocity at time $t + dt$ is

$$\mathbf{v}_I(t+dt) = \dot{\mathbf{R}}_I = \frac{\mathbf{R}_I(t+dt)-\mathbf{R}_I(t-dt)}{2\,dt}. \tag{5}$$

B. Average-atom molecular dynamics

We compare the EOS obtained from QLMD with the AAMD and OFMD simulations at typical density–temperature state points. In AAMD, the AA model is used to solve for the electron density, and

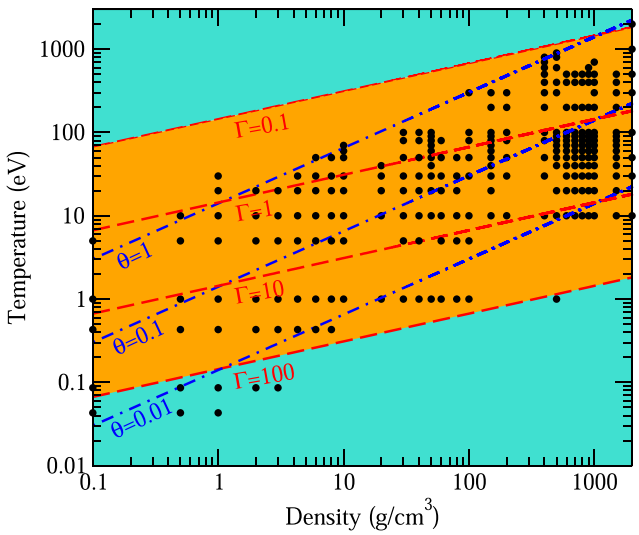

FIG. 1. Density–temperature state points chosen for EOS calculations for a DT mixture. The dashed lines for the coupling parameter $\Gamma = 0.1$, 1, and 10 and the dot-dashed lines for the degeneracy parameter $\theta = 0.01$, 0.1, and 1 are presented as guidelines.

then the modified temperature- and density-dependent Gordon–Kim (GK) theory is employed to obtain the ion–ion pair potential based on the electron density.[29,54] Finally, classical MD simulations are carried out for the ion motions. Specifically, we obtain the electron density by using a modified AA model to include the temperature and density effects on the electron distributions in a statistical manner.[27] The influence of the plasma environment on the atom is assumed to have spherical symmetry on average, and the occupation number of electrons on the orbitals of such a pseudo-atom is averaged over the possible ionic charge states. The electron orbitals of the ions are solved via the fully relativistic self-consistent-field Dirac equation

$$\frac{dP_{n\kappa}(r)}{dr} + \frac{\kappa}{r}P_{n\kappa}(r) = \frac{1}{c}[\epsilon_{n\kappa} + c^2 - V(r)]Q_{n\kappa}(r), \tag{6a}$$

$$\frac{dQ_{n\kappa}(r)}{dr} - \frac{\kappa}{r}Q_{n\kappa}(r) = -\frac{1}{c}[\epsilon_{n\kappa} - c^2 - V(r)]P_{n\kappa}(r), \tag{6b}$$

where $P_{n\kappa}(r)$ and $Q_{n\kappa}(r)$ are respectively the large and small components of the wave function. $V(r)$ is the self-consistent potential, which consists of static, exchange, and correlation potentials. Because the thermal fluctuations of ions in a plasma produce dynamic energy level broadening of the ions, Gaussian functions centered at the corresponding electron orbital energies are introduced into the Fermi–Dirac distribution of electrons. With this approach, the instability of the pressure-induced electronic ionization with density can be avoided in a natural manner.[27]

In the GK theory,[29,54] the total energy of a system includes the electrostatic Coulomb potential energy, the exchange potential energy, the correlation energy, and the kinetic energy. We construct a two-atom system, and the ion–ion pair interaction potential is then given by the difference in total energy between the coupled two-atom system and the two isolated-atom systems. It should be noted that at high temperatures, ionic many-body correlation effects will be very weak and can be neglected, and thus a pair potential is accurate enough to describe the ion correlations. However, at low temperatures, many-body correlations become important, and the pair-potential-based AAMD will deviate from *ab initio* methods.

C. Orbital-free molecular dynamics

The main difference between traditional QMD and OFMD is that the driving forces of the ions are obtained from two different DFT approaches: KSDFT and orbital-free DFT (OFDFT), respectively. In the framework of finite-temperature DFT,[33] the electron free energy is obtained by minimizing the grand canonical potential with respect to the electron density $n(\mathbf{r})$. The grand canonical potential has the form[43]

$$\Omega[n] = F[n] + \int d\mathbf{r}\,[v(\mathbf{r}) - \mu]n(\mathbf{r}), \tag{7}$$

where $v(\mathbf{r})$ is the external potential acting on the electrons corresponding to the density n, and μ is the chemical potential. The free energy functional $F[n]$ is composed of the noninteracting free energy $F_s[n]$, the classical Coulomb repulsion energy (i.e., Hartree energy) $F_H[n]$, and the exchange-correlation free energy $F_{xc}[n]$,

$$F[n] = F_s[n] + F_H[n] + F_{xc}[n]. \tag{8}$$

In conventional KSDFT, a sophisticated scheme exploits the one-electron orbitals of the noninteracting system to construct the electron density of the real system and thereby the total free energy. The advantage of KSDFT is that the noninteracting free energy functionals $F_s[n]$ can be constructed exactly from the one-electron orbitals and electron Fermi–Dirac occupations, thereby giving an explicit Euler equation once a suitable approximate F_{xc} is provided.

In contrast to conventional KSDFT, in OFDFT, the noninteracting functionals $T_s[n]$ and $S_s[n]$ are formulated directly in terms of the electron density rather than the KS orbitals. Minimization of the grand canonical potential in Eq. (7) with respect to the electron density $n(\mathbf{r})$ then gives the Euler–Lagrange equation

$$\frac{\delta T_s[n]}{\delta n} - T\frac{\delta S_s[n]}{\delta n} + \frac{\delta F_H[n]}{\delta n} + \frac{\delta F_{xc}[n]}{\delta n} = \mu - v(\mathbf{r}). \quad (9)$$

The computational cost of solving this equation scales linearly with the system size and is essentially independent of temperature. The accuracy of OFMD is largely determined by the quality of the noninteracting free energy functional.

III. RESULTS AND DISCUSSION

A. Computational details

We performed extensive calculations for the EOS of a DT mixture over wide ranges of temperature and density for ICF applications. The density–temperature state points chosen in this work are shown in Fig. 1. The density ranges from 0.1 g/cm^3 to 2000 g/cm^3 and the temperature from 500 K to 2000 eV. Regarding density and temperature, we can use two parameters, namely, the ion coupling parameter $\Gamma = Z^{*2}/(k_B T a)$ and the electron degeneracy parameter $\theta = T/T_F$, to define states of matter,[55] where Z^* is the average degree of ionization, T is the temperature, k_B is Boltzmann's constant, $a = [3/(4\pi n_i)]^{1/3}$ is the mean ion sphere radius, $T_F = (3\pi^2 n_e)^{2/3}/2$ is the Fermi temperature, n_e is the electron number density, and n_i is the ion number density. When the values of θ and Γ are close to 1, matter is in a partially degenerate and moderately coupled state. When $\theta \ll 1$, matter is strongly degenerate; conversely, it is weakly degenerate when $\theta \gg 1$. Matter is strongly or weakly coupled when the coupling parameter $\Gamma \gg 1$ or $\Gamma \ll 1$, respectively. As shown in Fig. 1, the coupling parameter Γ corresponding to the state points in this work is greater than 0.1, and most of the state points have $\Gamma \sim 1$ or $\gg 1$. Thus, the DT ions in the ICF process are in states ranging from moderately to strongly coupled. The degeneracy parameter θ corresponding to most of the state points is between 0.01 and 1. Thus, the electrons of DT are partially in strongly degenerate states.

We performed QLMD simulations using our locally modified version of the Quantum-ESPRESSO package.[56] The generalized gradient approximation in the Perdew–Burke–Ernzerhof parametrization[57] was used to treat the electron exchange-correlation functional. A norm-conserving pseudopotential was used in low-density conditions and a Coulomb pseudopotential with a cutoff radius of 0.005 a.u. was used in high-density conditions. The plane-wave cutoff energy was from 100 Ry to 1000 Ry, depending on the temperature and density. In the finite-temperature DFT framework, electrons occupy orbitals according to the Fermi–Dirac distribution. We included sufficient energy bands to ensure that the highest occupied band energy was higher than the chemical potential by at least $10k_BT$. Owing to the high computational efficiency of QLMD simulations resulting from the large self-consistent field tolerance, we can extend the QLMD simulation to extremely high temperatures at affordable computational cost. We used a supercell including 128–432 atoms, depending on the density. The mixing ratio of D and T atoms was 1:1. The Γ point was used to sample the Brillouin zone in the MD simulations. Convergence test calculations with denser k-point grids and larger supercells did not show any significant variations in the EOS data. The relative error was ~1% for pressure and 5 meV/atom for energy. For thermodynamic statistics, 2000–5000 steps after thermalization, with time steps of 0.02 fs–1 fs, were used.

In the OFMD calculations, the finite-temperature Thomas–Fermi noninteracting free energy functional with the von Weizsäcker density gradient correction (TFVW)[58,59] was used. The Perdew–Burke–Ernzerhof parameterized generalized gradient approximation functional was adopted for the electronic exchange-correlation interaction. A local pseudopotential was employed in all OFMD calculations.[43] The numerical grid for real-space integrations was set to $96 \times 96 \times 96$ to ensure convergence of the free energy and pressure. All the OFMD calculations were performed with our locally modified version of PROFESS.[60]

B. Comparison of different methods

A well-known *ab initio* EOS table of deuterium for ICF applications was derived by Hu *et al.*[6] using PIMC simulations. In Table I, we compare the QLMD results with the PIMC data. We select ten density–temperature points for comparison. It can be seen that the QLMD results are in good agreement with the PIMC data. The pressures obtained from QLMD simulations are slightly lower than those from PIMC simulations at low temperatures. At high temperatures, however, the opposite trend is seen. It was recently demonstrated that the remarkable agreement of QMD simulations with the experimental first-shock Hugoniot of deuterium arises from a cancellation of errors in the DFT model, whereas many-body methods like CEIMC can introduce non-negligible and additive errors into the evaluation of the Hugoniot curve.[41] This reminds us that in order to obtain more accurate EOS data, it is necessary to continuously reduce the size of the approximations in either the DFT model or the PIMC simulations.

TABLE I. Comparison of pressure between QLMD calculations and *ab initio* KSDFT-MD and PIMC calculations from Hu *et al.*[6]

r_s (bohr)	T (K)	P_{QLMD} (Mbar)	P_{Hu} (Mbar)
1.5	31 250	3.98	4.67
1.5	62 500	7.08	7.24
1.5	95 250	10.67	10.53
1.5	125 000	14.03	13.68
1.0	95 250	51.5	51.9
1.0	125 000	62.0	61.1
1.0	181 825	83.0	81.8
1.0	250 000	109.6	105.4
0.5	400 000	2152	2212
0.5	500 000	2430	2523

We also make a direct comparison of pressures obtained from these methods to show the applicability of AAMD and OFMD. We can see from Fig. 2 that at densities of 10 g/cm^3 and 100 g/cm^3, the pressures obtained from AAMD and OFMD simulations are in good agreement with those from QLMD in the temperature range from 1 eV to 300 eV, although the AAMD result is slightly higher than that from the QLMD calculation at 1 eV. In contrast to what is found at the densities of 10 g/cm^3 and 100 g/cm^3, when the density is as low as 4.3 g/cm^3 and 1 g/cm^3, the pressures exhibit large differences with decreasing temperature. The pressures from AAMD are remarkably larger than those from QLMD at temperatures below 10 eV. We note that the calculation of the electronic structure in AAMD employs a statistical single-atom model for ions in the plasma environment, and it neglects the correlation effects of ions, which play significant roles in the warm dense regime.[30] Therefore, AAMD gives inaccurate EOS data in the strong-coupling regime. From the comparisons between QLMD and OFMD results, we can see that OFMD performs better than AAMD. However, the pressures obtained from OFMD at 1 g/cm^3 and 4.3 g/cm^3 are higher than those from QLMD, especially at low temperatures (<1 eV). This is a consequence of the inability of OFMD to provide satisfactory descriptions of the shell structure of bound electrons and the chemical bond, and therefore OFMD becomes invalid at relatively low temperatures. Moreover, it should be noted that the pressure from OFMD is strongly dependent on the choice of noninteracting free energy functional.[61,62] The accuracy of the noninteracting free energy functional in OFMD simulations plays a critical role in calculations of the thermodynamic properties of matter under extreme conditions.

To gain further insight into the differences between AAMD, OFMD, and QLMD, we compare the radial distribution function (RDF) between these simulations for a DT mixture at 1 g/cm^3. Temperatures of 1000 K, 1 eV, and 5 eV are chosen for comparison. The results are presented in Fig. 3. We can see that at both 1000 K and 1 eV, the RDFs of DD, DT, and TT exhibit significant differences between AAMD, OFMD, and QLMD. When the temperature is as low as 1000 K, the RDFs obtained from QLMD have distinct peaks at 0.740 Å, 0.735 Å, and 0.725 Å for DD, TT, and DT, respectively. This means that there are a large number of molecules in QLMD simulations. By contrast, there are no molecular peaks of the RDFs in the OFMD simulations, which indicates that the DT mixture is in a dissociated atomic state in these simulations. The RDFs obtained from AAMD are similar to those from OFMD, although the first peaks are more structured in the case of AAMD. When the temperature is increased to 1 eV, there are still remarkable shoulders at about 0.9 Å in the QLMD simulations, indicating that there exist somewhat softened molecular structures. At 1 eV, the RDFs obtained both from AAMD and from OFMD show the distinct characteristics of atomic states, which is due to the fact that OFMD and AAMD cannot satisfactorily describe the bond formation in hydrogen molecules at low temperatures. When the temperature is increased to 5 eV, the RDFs obtained from three methods exhibit similar behavior, although there are still slight differences at the rising edge. At 5 eV, molecules have dissociated completely, and thus the spatial distributions of ions are in better agreement. From these comparisons, we can conclude that AAMD is accurate for hot dense DT mixtures and OFMD can be applied for calculating EOS data of DT mixtures over wider ranges of density and temperature than AAMD. However, neither of these two methods can provide accurate bonding

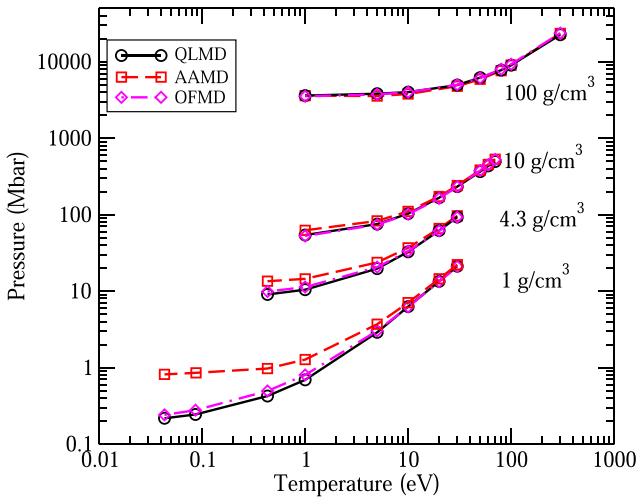

FIG. 2. Comparisons of pressure between QLMD, AAMD, and OFMD simulations at different densities.

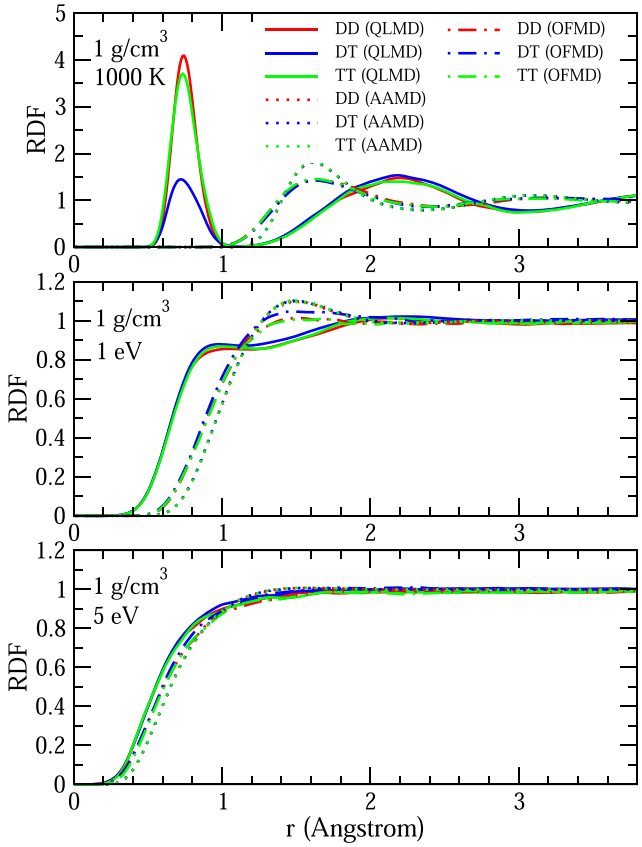

FIG. 3. Comparisons of RDF between AAMD, QLMD, and OFMD simulations at different temperatures.

TABLE II. Pressure and internal energy of DT mixture obtained from QLMD simulations. The mixing ratio of the D and T atoms is 1:1.

ρ (g/cm^3)	T (eV)	P (Mbar)	E (eV/atom)
0.1	0.0431	$0.830\,630 \times 10^{-3}$	$0.893\,764 \times 10^{-1}$
0.1	0.0862	$0.208\,015 \times 10^{-2}$	$0.159\,480 \times 10^{0}$
0.1	0.4309	$0.159\,371 \times 10^{-1}$	$0.738\,088 \times 10^{0}$
0.1	1	$0.464\,277 \times 10^{-1}$	$0.286\,924 \times 10^{1}$
0.1	5	$0.265\,759 \times 10^{0}$	$0.156\,949 \times 10^{2}$
0.5	0.0431	$0.292\,202 \times 10^{-1}$	$0.296\,166 \times 10^{-1}$
0.5	0.0862	$0.472\,310 \times 10^{-1}$	$0.170\,432 \times 10^{0}$
0.5	0.4309	$0.118\,262 \times 10^{0}$	$0.857\,053 \times 10^{0}$
0.5	1	$0.241\,796 \times 10^{0}$	$0.253\,468 \times 10^{1}$
0.5	5	$0.131\,360 \times 10^{1}$	$0.125\,735 \times 10^{2}$
0.5	10	$0.303\,850 \times 10^{1}$	$0.205\,336 \times 10^{2}$
1.0	0.0431	$0.217\,280 \times 10^{0}$	$0.221\,752 \times 10^{0}$
1.0	0.0862	$0.243\,720 \times 10^{0}$	$0.326\,576 \times 10^{0}$
1.0	0.4309	$0.424\,218 \times 10^{0}$	$0.133\,333 \times 10^{1}$
1.0	1	$0.690\,078 \times 10^{0}$	$0.260\,704 \times 10^{1}$
1.0	5	$0.289\,034 \times 10^{1}$	$0.118\,370 \times 10^{2}$
1.0	10	$0.627\,545 \times 10^{1}$	$0.218\,182 \times 10^{2}$
1.0	20	$0.133\,908 \times 10^{2}$	$0.553\,765 \times 10^{2}$
1.0	30	$0.211\,625 \times 10^{2}$	$0.868\,661 \times 10^{2}$
2.0	0.0862	$0.126\,027 \times 10^{1}$	$0.505\,120 \times 10^{0}$
2.0	0.4309	$0.160\,740 \times 10^{1}$	$0.120\,571 \times 10^{1}$
2.0	1	$0.218\,573 \times 10^{1}$	$0.226\,142 \times 10^{1}$
2.0	5	$0.669\,054 \times 10^{1}$	$0.109\,127 \times 10^{2}$
2.0	10	$0.130\,848 \times 10^{2}$	$0.238\,711 \times 10^{2}$
2.0	20	$0.266\,271 \times 10^{2}$	$0.514\,801 \times 10^{2}$
3.0	0.0862	$0.347\,879 \times 10^{1}$	$0.135\,113 \times 10^{1}$
3.0	0.4309	$0.406\,601 \times 10^{1}$	$0.204\,982 \times 10^{1}$
3.0	1	$0.500\,941 \times 10^{1}$	$0.315\,576 \times 10^{1}$
3.0	5	$0.115\,348 \times 10^{2}$	$0.114\,898 \times 10^{2}$
3.0	10	$0.209\,633 \times 10^{2}$	$0.240\,219 \times 10^{2}$
3.0	20	$0.412\,407 \times 10^{2}$	$0.513\,723 \times 10^{2}$
4.3	0.4309	$0.903\,747 \times 10^{1}$	$0.323\,160 \times 10^{1}$
4.3	1	$0.104\,389 \times 10^{2}$	$0.566\,524 \times 10^{1}$
4.3	5	$0.196\,980 \times 10^{2}$	$0.145\,167 \times 10^{2}$
4.3	10	$0.326\,685 \times 10^{2}$	$0.255\,680 \times 10^{2}$
4.3	20	$0.619\,302 \times 10^{2}$	$0.455\,667 \times 10^{2}$
4.3	30	$0.930\,045 \times 10^{2}$	$0.739\,879 \times 10^{2}$
6.0	0.4309	$0.182\,148 \times 10^{2}$	$0.542\,315 \times 10^{1}$
6.0	1	$0.200\,878 \times 10^{2}$	$0.656\,613 \times 10^{1}$
6.0	5	$0.329\,577 \times 10^{2}$	$0.148\,466 \times 10^{2}$
6.0	10	$0.510\,709 \times 10^{2}$	$0.268\,127 \times 10^{2}$
6.0	20	$0.897\,147 \times 10^{2}$	$0.505\,911 \times 10^{2}$
6.0	30	$0.131\,459 \times 10^{3}$	$0.785\,104 \times 10^{2}$
6.0	50	$0.213\,198 \times 10^{3}$	$0.134\,983 \times 10^{3}$
8.0	0.4309	$0.326\,272 \times 10^{2}$	$0.785\,861 \times 10^{1}$
8.0	1	$0.353\,270 \times 10^{2}$	$0.910\,206 \times 10^{1}$
8.0	5	$0.518\,475 \times 10^{2}$	$0.171\,658 \times 10^{2}$
8.0	10	$0.744\,856 \times 10^{2}$	$0.283\,626 \times 10^{2}$
8.0	20	$0.125\,218 \times 10^{3}$	$0.536\,383 \times 10^{2}$
8.0	30	$0.181\,336 \times 10^{3}$	$0.818\,916 \times 10^{2}$
8.0	50	$0.290\,176 \times 10^{3}$	$0.136\,064 \times 10^{3}$
10	1	$0.541\,138 \times 10^{2}$	$0.121\,455 \times 10^{2}$
10	5	$0.752\,248 \times 10^{2}$	$0.203\,847 \times 10^{2}$
10	10	$0.103\,092 \times 10^{3}$	$0.314\,908 \times 10^{2}$
10	20	$0.166\,441 \times 10^{3}$	$0.559\,489 \times 10^{2}$
10	30	$0.232\,817 \times 10^{3}$	$0.832\,438 \times 10^{2}$
10	50	$0.365\,237 \times 10^{3}$	$0.143\,951 \times 10^{3}$
10	60	$0.434\,460 \times 10^{3}$	$0.171\,941 \times 10^{3}$
10	70	$0.495\,289 \times 10^{3}$	$0.199\,242 \times 10^{3}$
20	1	$0.198\,640 \times 10^{3}$	$0.247\,073 \times 10^{2}$
20	10	$0.293\,952 \times 10^{3}$	$0.438\,820 \times 10^{2}$
20	20	$0.403\,253 \times 10^{3}$	$0.652\,815 \times 10^{2}$
20	30	$0.504\,169 \times 10^{3}$	$0.844\,459 \times 10^{2}$
20	40	$0.651\,612 \times 10^{3}$	$0.110\,604 \times 10^{3}$
30	1	$0.417\,386 \times 10^{3}$	$0.310\,208 \times 10^{2}$
30	5	$0.481\,431 \times 10^{3}$	$0.396\,813 \times 10^{2}$
30	10	$0.558\,413 \times 10^{3}$	$0.501\,033 \times 10^{2}$
30	20	$0.719\,670 \times 10^{3}$	$0.716\,645 \times 10^{2}$
30	30	$0.897\,887 \times 10^{3}$	$0.953\,480 \times 10^{2}$
30	50	$0.128\,260 \times 10^{4}$	$0.146\,395 \times 10^{3}$
30	80	$0.189\,396 \times 10^{4}$	$0.227\,263 \times 10^{3}$
30	100	$0.228\,661 \times 10^{4}$	$0.279\,111 \times 10^{3}$
40	1	$0.702\,601 \times 10^{3}$	$0.423\,181 \times 10^{2}$
40	5	$0.788\,859 \times 10^{3}$	$0.511\,872 \times 10^{2}$
40	10	$0.890\,611 \times 10^{3}$	$0.615\,825 \times 10^{2}$
40	20	$0.110\,025 \times 10^{4}$	$0.827\,591 \times 10^{2}$
40	30	$0.132\,767 \times 10^{4}$	$0.105\,468 \times 10^{3}$
40	50	$0.182\,875 \times 10^{4}$	$0.155\,348 \times 10^{3}$
40	80	$0.263\,455 \times 10^{4}$	$0.235\,454 \times 10^{3}$
40	100	$0.317\,228 \times 10^{4}$	$0.288\,630 \times 10^{3}$
50	1	$0.105\,061 \times 10^{4}$	$0.589\,545 \times 10^{2}$
50	10	$0.128\,182 \times 10^{4}$	$0.779\,803 \times 10^{2}$
50	20	$0.154\,161 \times 10^{4}$	$0.991\,708 \times 10^{2}$
50	30	$0.181\,325 \times 10^{4}$	$0.121\,028 \times 10^{3}$
50	40	$0.211\,662 \times 10^{4}$	$0.145\,931 \times 10^{3}$
50	50	$0.245\,074 \times 10^{4}$	$0.172\,317 \times 10^{3}$
50	60	$0.269\,388 \times 10^{4}$	$0.197\,413 \times 10^{3}$
50	70	$0.310\,001 \times 10^{4}$	$0.223\,775 \times 10^{3}$
50	80	$0.337\,949 \times 10^{4}$	$0.244\,219 \times 10^{3}$
50	90	$0.373\,639 \times 10^{4}$	$0.272\,966 \times 10^{3}$
50	100	$0.402\,437 \times 10^{4}$	$0.291\,582 \times 10^{3}$
60	1	$0.145\,557 \times 10^{4}$	$0.637\,770 \times 10^{2}$
60	5	$0.158\,439 \times 10^{4}$	$0.727\,918 \times 10^{2}$
60	10	$0.173\,756 \times 10^{4}$	$0.833\,327 \times 10^{2}$
60	20	$0.203\,882 \times 10^{4}$	$0.103\,714 \times 10^{3}$
60	30	$0.236\,227 \times 10^{4}$	$0.125\,379 \times 10^{3}$
60	50	$0.308\,837 \times 10^{4}$	$0.173\,926 \times 10^{3}$
60	80	$0.424\,276 \times 10^{4}$	$0.249\,837 \times 10^{3}$
80	1	$0.242\,667 \times 10^{4}$	$0.737\,350 \times 10^{2}$
80	5	$0.259\,989 \times 10^{4}$	$0.829\,814 \times 10^{2}$
80	10	$0.280\,119 \times 10^{4}$	$0.934\,068 \times 10^{2}$
80	20	$0.320\,109 \times 10^{4}$	$0.113\,876 \times 10^{3}$
80	30	$0.361\,744 \times 10^{4}$	$0.134\,881 \times 10^{3}$
80	50	$0.455\,277 \times 10^{4}$	$0.182\,058 \times 10^{3}$
100	1	$0.360\,545 \times 10^{4}$	$0.108\,789 \times 10^{3}$

TABLE II. (*Continued.*)

ρ (g/cm^3)	T (eV)	P (Mbar)	E (eV/atom)
100	5	$0.381\,778 \times 10^4$	$0.117\,996 \times 10^3$
100	10	$0.400\,615 \times 10^4$	$0.126\,345 \times 10^3$
100	30	$0.495\,574 \times 10^4$	$0.162\,966 \times 10^3$
100	50	$0.620\,446 \times 10^4$	$0.210\,407 \times 10^3$
100	80	$0.775\,170 \times 10^4$	$0.272\,019 \times 10^3$
100	100	$0.901\,808 \times 10^4$	$0.320\,191 \times 10^3$
100	300	$0.225\,540 \times 10^5$	$0.852\,509 \times 10^3$
150	10	$0.805\,511 \times 10^4$	$0.173\,198 \times 10^3$
150	20	$0.878\,961 \times 10^4$	$0.193\,462 \times 10^3$
150	30	$0.951\,154 \times 10^4$	$0.213\,229 \times 10^3$
150	40	$0.102\,731 \times 10^5$	$0.233\,401 \times 10^3$
150	50	$0.110\,512 \times 10^5$	$0.254\,745 \times 10^3$
150	60	$0.119\,259 \times 10^5$	$0.277\,811 \times 10^3$
150	70	$0.127\,475 \times 10^5$	$0.299\,820 \times 10^3$
150	80	$0.136\,931 \times 10^5$	$0.325\,343 \times 10^3$
150	90	$0.145\,807 \times 10^5$	$0.348\,694 \times 10^3$
150	100	$0.155\,280 \times 10^5$	$0.373\,042 \times 10^3$
150	200	$0.256\,413 \times 10^5$	$0.639\,960 \times 10^3$
150	300	$0.362\,915 \times 10^5$	$0.920\,057 \times 10^3$
200	10	$0.130\,680 \times 10^5$	$0.214\,326 \times 10^3$
200	30	$0.146\,931 \times 10^5$	$0.255\,231 \times 10^3$
200	50	$0.170\,607 \times 10^5$	$0.296\,192 \times 10^3$
200	80	$0.202\,755 \times 10^5$	$0.359\,368 \times 10^3$
200	100	$0.226\,732 \times 10^5$	$0.407\,772 \times 10^3$
200	200	$0.359\,308 \times 10^5$	$0.671\,268 \times 10^3$
200	300	$0.499\,215 \times 10^5$	$0.947\,821 \times 10^3$
400	10	$0.421\,921 \times 10^5$	$0.357\,649 \times 10^3$
400	30	$0.457\,385 \times 10^5$	$0.393\,904 \times 10^3$
400	50	$0.494\,821 \times 10^5$	$0.432\,096 \times 10^3$
400	80	$0.558\,434 \times 10^5$	$0.497\,470 \times 10^3$
400	100	$0.601\,729 \times 10^5$	$0.540\,605 \times 10^3$
400	200	$0.844\,886 \times 10^5$	$0.784\,326 \times 10^3$
400	300	$0.110\,634 \times 10^6$	$0.103\,987 \times 10^4$
400	400	$0.137\,026 \times 10^6$	$0.129\,070 \times 10^4$
400	500	$0.166\,671 \times 10^6$	$0.159\,119 \times 10^4$
400	600	$0.196\,346 \times 10^6$	$0.188\,826 \times 10^4$
400	700	$0.225\,036 \times 10^6$	$0.216\,509 \times 10^4$
400	800	$0.254\,658 \times 10^6$	$0.245\,899 \times 10^4$
500	1	$0.592\,628 \times 10^5$	$0.402\,215 \times 10^3$
500	10	$0.615\,391 \times 10^5$	$0.422\,430 \times 10^3$
500	20	$0.639\,539 \times 10^5$	$0.442\,209 \times 10^3$
500	40	$0.688\,266 \times 10^5$	$0.483\,048 \times 10^3$
500	50	$0.712\,705 \times 10^5$	$0.502\,776 \times 10^3$
500	60	$0.734\,843 \times 10^5$	$0.522\,595 \times 10^3$
500	70	$0.759\,346 \times 10^5$	$0.540\,824 \times 10^3$
500	80	$0.785\,441 \times 10^5$	$0.562\,702 \times 10^3$
500	90	$0.811\,220 \times 10^5$	$0.582\,423 \times 10^3$
500	100	$0.834\,765 \times 10^5$	$0.602\,426 \times 10^3$
500	300	$0.144\,253 \times 10^6$	$0.108\,198 \times 10^4$
500	400	$0.175\,729 \times 10^6$	$0.131\,825 \times 10^4$
500	600	$0.250\,266 \times 10^6$	$0.191\,981 \times 10^4$
500	800	$0.319\,268 \times 10^6$	$0.249\,025 \times 10^4$

TABLE II. (*Continued.*)

ρ (g/cm^3)	T (eV)	P (Mbar)	E (eV/atom)
500	900	$0.359\,672 \times 10^6$	$0.277\,933 \times 10^4$
600	10	$0.824\,551 \times 10^5$	$0.472\,746 \times 10^3$
600	20	$0.852\,799 \times 10^5$	$0.493\,154 \times 10^3$
600	30	$0.880\,921 \times 10^5$	$0.512\,682 \times 10^3$
600	40	$0.909\,708 \times 10^5$	$0.532\,390 \times 10^3$
600	50	$0.940\,306 \times 10^5$	$0.554\,167 \times 10^3$
600	60	$0.967\,949 \times 10^5$	$0.571\,934 \times 10^3$
600	70	$0.998\,670 \times 10^5$	$0.592\,776 \times 10^3$
600	80	$0.102\,715 \times 10^6$	$0.611\,417 \times 10^3$
600	90	$0.105\,698 \times 10^6$	$0.631\,554 \times 10^3$
600	100	$0.109\,081 \times 10^6$	$0.654\,774 \times 10^3$
600	200	$0.142\,588 \times 10^6$	$0.877\,112 \times 10^3$
600	400	$0.221\,150 \times 10^6$	$0.139\,394 \times 10^4$
600	500	$0.263\,333 \times 10^6$	$0.167\,003 \times 10^4$
700	10	$0.107\,065 \times 10^6$	$0.529\,407 \times 10^3$
700	20	$0.110\,244 \times 10^6$	$0.548\,872 \times 10^3$
700	30	$0.113\,508 \times 10^6$	$0.568\,463 \times 10^3$
700	40	$0.116\,879 \times 10^6$	$0.588\,468 \times 10^3$
700	50	$0.120\,301 \times 10^6$	$0.609\,458 \times 10^3$
700	60	$0.123\,842 \times 10^6$	$0.630\,543 \times 10^3$
700	70	$0.127\,294 \times 10^6$	$0.649\,902 \times 10^3$
700	80	$0.130\,446 \times 10^6$	$0.667\,672 \times 10^3$
700	90	$0.134\,124 \times 10^6$	$0.689\,083 \times 10^3$
700	100	$0.138\,138 \times 10^6$	$0.712\,666 \times 10^3$
700	200	$0.176\,204 \times 10^6$	$0.927\,304 \times 10^3$
700	400	$0.266\,514 \times 10^6$	$0.143\,925 \times 10^4$
700	500	$0.314\,516 \times 10^6$	$0.171\,003 \times 10^4$
800	10	$0.134\,187 \times 10^6$	$0.583\,366 \times 10^3$
800	20	$0.137\,943 \times 10^6$	$0.603\,970 \times 10^3$
800	30	$0.141\,636 \times 10^6$	$0.623\,423 \times 10^3$
800	40	$0.145\,631 \times 10^6$	$0.644\,979 \times 10^3$
800	50	$0.149\,328 \times 10^6$	$0.663\,649 \times 10^3$
800	60	$0.153\,409 \times 10^6$	$0.685\,324 \times 10^3$
800	70	$0.157\,280 \times 10^6$	$0.704\,522 \times 10^3$
800	80	$0.161\,125 \times 10^6$	$0.723\,688 \times 10^3$
800	90	$0.165\,350 \times 10^6$	$0.746\,691 \times 10^3$
800	100	$0.169\,045 \times 10^6$	$0.765\,223 \times 10^3$
800	200	$0.213\,167 \times 10^6$	$0.984\,776 \times 10^3$
800	400	$0.313\,743 \times 10^6$	$0.148\,189 \times 10^4$
800	500	$0.367\,831 \times 10^6$	$0.174\,929 \times 10^4$
900	10	$0.163\,903 \times 10^6$	$0.636\,570 \times 10^3$
900	20	$0.168\,094 \times 10^6$	$0.656\,813 \times 10^3$
900	30	$0.172\,127 \times 10^6$	$0.675\,542 \times 10^3$
900	40	$0.176\,287 \times 10^6$	$0.694\,598 \times 10^3$
900	50	$0.180\,864 \times 10^6$	$0.716\,326 \times 10^3$
900	60	$0.185\,036 \times 10^6$	$0.735\,248 \times 10^3$
900	70	$0.189\,782 \times 10^6$	$0.757\,299 \times 10^3$
900	80	$0.194\,191 \times 10^6$	$0.777\,325 \times 10^3$
900	90	$0.198\,990 \times 10^6$	$0.798\,916 \times 10^3$
900	100	$0.203\,012 \times 10^6$	$0.816\,659 \times 10^3$
900	200	$0.250\,805 \times 10^6$	$0.102\,664 \times 10^4$
900	400	$0.363\,881 \times 10^6$	$0.152\,672 \times 10^4$

TABLE II. (*Continued.*)

ρ (g/cm^3)	T (eV)	P (Mbar)	E (eV/atom)
900	500	$0.424\,034 \times 10^6$	$0.178\,798 \times 10^4$
900	600	$0.485\,994 \times 10^6$	$0.205\,993 \times 10^4$
1000	10	$0.196\,137 \times 10^6$	$0.688\,637 \times 10^3$
1000	20	$0.200\,572 \times 10^6$	$0.707\,797 \times 10^3$
1000	30	$0.205\,116 \times 10^6$	$0.726\,987 \times 10^3$
1000	40	$0.209\,798 \times 10^6$	$0.746\,911 \times 10^3$
1000	50	$0.214\,735 \times 10^6$	$0.768\,303 \times 10^3$
1000	60	$0.219\,515 \times 10^6$	$0.787\,275 \times 10^3$
1000	70	$0.224\,192 \times 10^6$	$0.804\,680 \times 10^3$
1000	80	$0.228\,979 \times 10^6$	$0.825\,465 \times 10^3$
1000	90	$0.234\,152 \times 10^6$	$0.846\,817 \times 10^3$
1000	100	$0.239\,005 \times 10^6$	$0.864\,189 \times 10^3$
1000	200	$0.289\,583 \times 10^6$	$0.106\,906 \times 10^4$
1000	300	$0.347\,559 \times 10^6$	$0.129\,872 \times 10^4$
1000	400	$0.399\,541 \times 10^6$	$0.149\,109 \times 10^4$
1000	500	$0.465\,088 \times 10^6$	$0.176\,053 \times 10^4$
1000	700	$0.618\,038 \times 10^6$	$0.236\,502 \times 10^4$
1500	10	$0.390\,805 \times 10^5$	$0.926\,828 \times 10^3$
1500	20	$0.397\,952 \times 10^6$	$0.947\,931 \times 10^3$
1500	30	$0.405\,044 \times 10^6$	$0.968\,592 \times 10^3$
1500	40	$0.411\,886 \times 10^6$	$0.988\,016 \times 10^3$
1500	50	$0.418\,707 \times 10^6$	$0.100\,780 \times 10^4$
1500	60	$0.425\,154 \times 10^6$	$0.102\,478 \times 10^4$
1500	70	$0.432\,483 \times 10^6$	$0.104\,628 \times 10^4$
1500	80	$0.439\,258 \times 10^6$	$0.106\,480 \times 10^4$
1500	90	$0.446\,302 \times 10^6$	$0.108\,313 \times 10^4$
1500	100	$0.453\,229 \times 10^6$	$0.110\,064 \times 10^4$
1500	200	$0.528\,935 \times 10^6$	$0.130\,170 \times 10^4$
1500	300	$0.610\,289 \times 10^6$	$0.151\,908 \times 10^4$
1500	400	$0.701\,521 \times 10^6$	$0.175\,979 \times 10^4$
1500	500	$0.794\,686 \times 10^6$	$0.200\,413 \times 10^4$
2000	10	$0.595\,386 \times 10^6$	$0.110\,960 \times 10^4$
2000	30	$0.613\,423 \times 10^6$	$0.115\,065 \times 10^4$
2000	50	$0.631\,282 \times 10^6$	$0.118\,863 \times 10^4$
2000	100	$0.675\,121 \times 10^6$	$0.128\,456 \times 10^4$
2000	300	$0.866\,001 \times 10^6$	$0.168\,119 \times 10^4$
2000	500	$0.108\,091 \times 10^7$	$0.212\,541 \times 10^4$
2000	1000	$0.166\,975 \times 10^7$	$0.331\,348 \times 10^4$
2000	2000	$0.314\,344 \times 10^7$	$0.541\,042 \times 10^4$

information for DT mixtures at relatively low temperatures. In comparison with AAMD and OFMD, QLMD which is based on an accurate description of electronic structure and an efficient MD algorithm, can provide accurate EOS data for DT mixtures from low-temperature condensed states to the hot dense regime.

C. EOS data

Table II shows the pressure and internal energy of DT mixtures obtained from QLMD simulations. The density ranges from 0.1 g/cm^3 to 2000 g/cm^3 and the temperature from 500 K to 2000 eV. Here, the total internal energy is obtained from

$$E = F - TS + E_{\mathrm{kin}}, \tag{10}$$

where F is the free energy of the simulation system obtained from the finite-temperature DFT self-consistent-field iterations, S is the entropy, T is the temperature, and E_{kin} is the kinetic energy of ions. The pressure is calculated from

$$P = nk_BT + P_{\mathrm{DFT}}, \tag{11}$$

where n is the ion number density, nk_BT is the ideal kinetic contribution of ions, and P_{DFT} is the interaction contribution calculated from DFT self-consistent-field iterations, which includes contributions from the kinetic energy of electrons, the ion–electron interaction, the Hartree interaction of electrons, and the electronic exchange-correlation interaction.

We should stress that the KSDFT calculations are still computationally expensive at high temperatures, even though QLMD lowers the convergence criteria of the self-consistent-field calculations. Therefore, 248 density–temperature state points are adopted to calculate the EOS of a DT mixture, as shown in Table II. These EOS data should be interpolated with a denser density–temperature grid set when applied to ICF hydrodynamic simulations. The interpolation approach can affect the accuracy of interpolated EOS data,[63] and therefore a proper interpolation method needs to be employed. However, this is outside the scope of this work. In addition, when the density of matter is extremely high and the temperature is relatively low, nuclear quantum effects become significant for atomic structures, transport properties, and thermodynamic properties, especially in the case of light elements such as hydrogen.[64,65] We can use a parameter α, which is defined as the ratio of the ionic thermal de Broglie wavelength to the mean distance between ions, to measure the degree to which the ions exhibit a quantum nature. For all the densities and temperatures considered here, α is less than 0.3. In terms of our previous investigations,[66] nuclear quantum effects play notable roles in static structures and thermodynamic properties only if $\alpha > 0.3$. Therefore, the quantum nature of the DT ions can be neglected in this work.

IV. CONCLUSIONS

We have performed extensive QLMD simulations to obtain EOS data for DT mixtures over wide ranges of density (from 0.1 g/cm^3 to 2000 g/cm^3) and temperature (from 500 K to 2000 eV) relevant to ICF implosions. Comparisons with AAMD and OFMD simulations reveal significant discrepancies at relatively low temperatures, where the strong ionic coupling plays a remarkable role in determining the EOS of DT mixtures. The DFT-based simulation methods provide more reliable EOS data than previous semiclassical methods. In the future, we should pay special attention to basic physical issues such as electronic many-body effects and nonlocal interactions[65] to meet the requirements for higher-precision EOS data not only for ICF applications, but also for planetary science and astrophysics.

ACKNOWLEDGMENTS

This work was supported by the Science Challenge Project under Grant No. TZ2016001, the National Key R&D Program of China under Grant No. 2017YFA0403200, the National Natural Science Foundation of China under Grant Nos. 11874424 and 11774429, and the NSAF under Grant No. U1830206. All calculations were carried out at the Research Center of Supercomputing Applications at NUDT.

REFERENCES

[1]E. M. Campbell, V. N. Goncharov, T. C. Sangster, S. P. Regan, P. B. Radha *et al.*, "Laser-direct-drive program: Promise, challenge, and path forward," Matter Radiat. Extremes **2**, 37 (2017).

[2]Z. Li, Z. Wang, R. Xu, J. Yang, F. Ye *et al.*, "Experimental investigation of Z-pinch radiation source for indirect drive inertial confinement fusion," Matter Radiat. Extremes **4**, 046201 (2019).

[3]J. Lindl, "Development of the indirect-drive approach to inertial confinement fusion and the target physics basis for ignition and gain," Phys. Plasmas **2**, 3933 (1995).

[4]L. Caillabet, S. Mazevet, and P. Loubeyre, "Multiphase equation of state of hydrogen from ab initio calculations in the range 0.2 to 5 g/cc up to 10 eV," Phys. Rev. B **83**, 094101 (2011).

[5]L. Caillabet, B. Canaud, G. Salin, S. Mazevet, and P. Loubeyre, "Change in inertial confinement fusion implosions upon using an ab initio multiphase DT equation of state," Phys. Rev. Lett. **107**, 115004 (2011).

[6]S. X. Hu, B. Militzer, V. N. Goncharov, and S. Skupsky, "First-principles equation-of-state table of deuterium for inertial confinement fusion applications," Phys. Rev. B **84**, 224109 (2011).

[7]S. X. Hu, L. A. Collins, V. N. Goncharov, J. D. Kress, T. R. Boehly *et al.*, "First-principles studies on the equation of state, thermal conductivity, and opacity of deuterium-tritium (DT) and polystyrene (CH) for inertial confinement fusion applications," J. Phys.: Conf. Ser. **717**, 012064 (2016).

[8]J. Danel, L. Kazandjian, and R. Piron, "Equation of state of warm dense deuterium and its isotopes from density-functional theory molecular dynamics," Phys. Rev. E **93**, 043210 (2016).

[9]C. Wang and P. Zhang, "Wide range equation of state for fluid hydrogen from density functional theory," Phys. Plasmas **20**, 092703 (2013).

[10]M. A. Morales, L. X. Benedict, D. S. Clark, E. Schwegler, I. Tamblyn *et al.*, "Ab initio calculations of the equation of state of hydrogen in a regime relevant for inertial fusion applications," High Energy Density Phys. **8**, 5 (2012).

[11]H. Liu, G. Zhang, Q. Zhang, H. Song, Q. Li *et al.*, "Progress on equation of state of hydrogen and deuterium," Chin. J. High Pressure Phys. **32**, 050101 (2018).

[12]J. A. Gaffney, S. X. Hu, P. Arnault, A. Becker, L. X. Benedict *et al.*, "A review of equation-of-state models for inertial confinement fusion materials," High Energy Density Phys. **28**, 7 (2018).

[13]S. Faik, A. Tauschwitz, and I. Iosilevskiy, "The equation of state package FEOS for high energy density matter," Comput. Phys. Commun. **227**, 117 (2018).

[14]W. J. Nellis, "Dynamic compression of materials: Metallization of fluid hydrogen at high pressures," Rep. Prog. Phys. **69**, 1479 (2006).

[15]G. V. Boriskov, A. I. Bykov, R. Ilkaev, V. D. Selemir, G. V. Simakov *et al.*, "Shock compression of liquid deuterium up to 109 GPa," Phys. Rev. B **71**, 092104 (2005).

[16]D. G. Hicks, T. R. Boehly, P. M. Celliers, J. H. Eggert, S. J. Moon *et al.*, "Laser-driven single shock compression of fluid deuterium from 45 to 220 GPa," Phys. Rev. B **79**, 014112 (2009).

[17]R. Nora, W. Theobald, R. Betti, F. J. Marshall, D. T. Michel *et al.*, "Gigabar spherical shock generation on the OMEGA laser," Phys. Rev. Lett. **114**, 045001 (2015).

[18]A. Fernandez-Pañella, M. Millot, D. E. Fratanduono, M. P. Desjarlais, S. Hamel *et al.*, "Shock compression of liquid deuterium up to 1 TPa," Phys. Rev. Lett. **122**, 255702 (2019).

[19]M. D. Knudson, D. L. Hanson, J. E. Bailey, C. A. Hall, J. R. Asay *et al.*, "Principal hugoniot, reverberating wave, and mechanical reshock measurements of liquid deuterium to 400 GPa using plate impact techniques," Phys. Rev. B **69**, 144209 (2004).

[20]M. D. Knudson, M. P. Desjarlais, A. Becker, R. W. Lemke, K. R. Cochrance *et al.*, "Direct observation of an abrupt insulator-to-metal transition in dense liquid deuterium," Science **348**, 1455 (2015).

[21]D. Saumon and G. Chabrier, "Fluid hydrogen at high density: Pressure ionization," Phys. Rev. A **46**, 2084 (1992).

[22]F. J. Rogers, "New activity expansion calculations for warm dense deuterium," Contrib. Plasma Phys. **41**, 179 (2001).

[23]H. Juranek, R. Redmer, and Y. Rosenfeld, "Fluid variational theory for pressure dissociation in dense hydrogen: Multicomponent reference system and nonadditivity effects," J. Chem. Phys. **117**, 1768 (2002).

[24]V. K. Gryaznov, I. L. Iosilevskiy, and V. E. Fortov, "Thermodynamics of hydrogen and helium plasmas in megabar and multi-megabar pressure range under strong shock and isentropic compression," Plasma Phys. Controlled Fusion **58**, 014012 (2016).

[25]G. I. Kerley, "Equation of state and phase diagram of dense hydrogen," Phys. Earth Planet. Inter. **6**, 78 (1972).

[26]G. I. Kerley, Technical Report No. SAND2003-3613, Sandia National Laboratory, Albuquerque, NM, 2003.

[27]Y. Hou, F. Jin, and J. Yuan, "Influence of the electronic energy level broadening on the ionization of atoms in hot and dense plasmas: An average atom model demonstration," Phys. Plasmas **13**, 093301 (2006).

[28]J. Chihara, "Average atom model based on quantum hyper-netted chain method," High Energy Density Phys. **19**, 38 (2016).

[29]Y. Hou and J. Yuan, "Alternative ion-ion pair-potential model applied to molecular dynamics simulations of hot and dense plasmas: Al and Fe as examples," Phys. Rev. E **79**, 016402 (2009).

[30]S. X. Hu, B. Militzer, V. N. Goncharov, and S. Skupsky, "Strong coupling and degeneracy effects in inertial confinement fusion implosions," Phys. Rev. Lett. **104**, 235003 (2010).

[31]P. Hohenberg and W. Kohn, "Inhomogeneous electron gas," Phys. Rev. **136**, B864 (1964).

[32]W. Kohn and L. J. Sham, "Self-consistent equations including exchange and correlation effects," Phys. Rev. **140**, A1133 (1965).

[33]N. D. Mermin, "Thermal properties of the inhomogeneous electron gas," Phys. Rev. **137**, A1441 (1965).

[34]T. J. Lenosky, S. R. Bickham, J. D. Kress, and L. A. Collins, "Density-functional calculation of the Hugoniot of shocked liquid deuterium," Phys. Rev. B **61**, 1 (2000).

[35]M. P. Desjarlais, "Density-functional calculations of the liquid deuterium Hugoniot, reshock, and reverberation timing," Phys. Rev. B **68**, 064204 (2003).

[36]B. Holst, R. Redmer, and M. P. Desjarlais, "Thermophysical properties of warm dense hydrogen using quantum molecular dynamics simulations," Phys. Rev. B **77**, 184201 (2008).

[37]B. Militzer and D. M. Ceperley, "Path integral Monte Carlo calculation of the deuterium Hugoniot," Phys. Rev. Lett. **85**, 1890 (2000).

[38]K. P. Driver and B. Militzer, "All-electron path integral Monte Carlo simulations of warm dense matter: Application to water and carbon plasmas," Phys. Rev. Lett. **108**, 115502 (2012).

[39]C. Pierleoni, D. M. Ceperley, and M. Holzmann, "Coupled electron-ion Monte Carlo calculations of dense metallic hydrogen," Phys. Rev. Lett. **93**, 146402 (2004).

[40]M. A. Morales, C. Pierleoni, and D. M. Ceperley, "Equation of state of metallic hydrogen from coupled electron-ion Monte Carlo simulations," Phys. Rev. E **81**, 021202 (2010).

[41]R. C. Clay III, M. P. Desjarlais, and L. Shulenburger, "Deuterium Hugoniot: Pitfalls of thermodynamic sampling beyond density functional theory," Phys. Rev. B **100**, 075103 (2019).

[42]F. Lambert, J. Clérouin, and G. Zérah, "Very-high-temperature molecular dynamics," Phys. Rev. E **73**, 016403 (2006).

[43]V. V. Karasiev, T. Sjostrom, and S. B. Trickey, "Generalized-gradient-approximation noninteracting free-energy functionals for orbital-free density functional calculations," Phys. Rev. B **86**, 115101 (2012).

[44]H. Y. Sun, D. Kang, Y. Hou, and J. Y. Dai, "Transport properties of warm and hot dense iron from orbital free and corrected Yukawa potential molecular dynamics," Matter Radiat. Extremes **2**, 287 (2017).

[45]S. Zhang, H. Wang, W. Kang, P. Zhang, and X. T. He, "Extended application of Kohn–Sham first-principles molecular dynamics method with plane wave approximation at high energyąłFrom cold materials to hot dense plasmas," Phys. Plasmas **23**, 042707 (2016).

[46]J. Dai, Y. Hou, and J. Yuan, "Unified first principles description from warm dense matter to ideal ionized gas plasma: Electron-ion collisions induced friction," Phys. Rev. Lett. **104**, 245001 (2010).

[47]J. Dai and J. Yuan, "Large-scale efficient Langevin dynamics, and why it works," Europhys. Lett. **88**, 20001 (2009).
[48]J. Dai, Y. Hou, and J. Yuan, "Quantum Langevin molecular dynamic determination of the solar-interior equation of state," Astrophys. J. **721**, 1158 (2010).
[49]J. Dai, Y. Hou, and J. Yuan, "Influence of ordered structures on electrical conductivity and XANES from warm to hot dense matter," High Energy Density Phys. **7**, 84 (2011).
[50]J. Dai, D. Kang, Z. Zhao, Y. Wu, and J. Yuan, "Dynamic ionic clusters with flowing electron bubbles from warm to hot dense iron along the Hugoniot curve," Phys. Rev. Lett. **109**, 175701 (2012).
[51]J. Dai, Y. Hou, D. Kang, H. Sun, J. Wu *et al.*, "Structure, equation of state, diffusion and viscosity of warm dense Fe under the conditions of a giant planet core," New J. Phys. **15**, 045003 (2013).
[52]D. Kang and J. Dai, "Dynamic electron–cion collisions and nuclear quantum effects in quantum simulation of warm dense matter," J. Phys.: Condens. Matter **30**, 073002 (2018).
[53]A. V. Plyukhin, "Generalized Fokker-Planck equation, Brownian motion, and ergodicity," Phys. Rev. E **77**, 061136 (2008).
[54]R. G. Gordon and Y. S. Kim, "Theory for the forces between closed-shell atoms and molecules," J. Chem. Phys. **56**, 3122 (1972).
[55]S. Ichimaru, "Strongly coupled plasmas: High-density classical plasmas and degenerate electron liquids," Rev. Mod. Phys. **54**, 1017 (1982).
[56]P. Giannozzi, O. Andreussi, T. Brumme, O. Bunau, M. B. Nardelli *et al.*, "Advanced capabilities for materials modelling with quantum ESPRESSO," J. Phys.: Condens. Matter **29**, 465901 (2017).
[57]J. P. Perdew, K. Burke, and M. Ernzerhof, "Generalized gradient approximation made simple," Phys. Rev. Lett. **77**, 3865 (1996).
[58]R. P. Feynman, N. Metropolis, and E. Teller, "Equations of state of elements based on the generalized Fermi-Thomas theory," Phys. Rev. **75**, 1561 (1949).
[59]F. Perrot, "Gradient correction to the statistical electronic free energy at nonzero temperatures: Application to equation-of-state calculations," Phys. Rev. A **20**, 586 (1979).
[60]M. Chen, X. C. Huang, J. M. Dieterich, L. Hung, I. Shin *et al.*, "Introducing PROFESS 3.0: An advanced program for orbital-free density functional theory molecular dynamics simulations," Comput. Phys. Commun. **190**, 228 (2015).
[61]K. Luo, V. V. Karasiev, and S. B. Trickey, "A simple generalized gradient approximation for the noninteracting kinetic energy density functional," Phys. Rev. B **98**, 041111(R) (2018).
[62]K. Luo, V. V. Karasiev, and S. B. Trickey, "Towards accurate orbital-free simulations: A generalized gradient approximation for the noninteracting free energy density functional," Phys. Rev. B **101**, 075116 (2020).
[63]V. A. Baturin, W. Däppen, A. V. Oreshina, S. V. Ayukov, and A. B. Gorshkov, "Interpolation of equation-of-state data," Astron. Astrophys. **626**, A108 (2019).
[64]D. Kang, H. Sun, J. Dai, W. Chen, Z. Zhao *et al.*, "Nuclear quantum dynamics in dense hydrogen," Sci. Rep. **4**, 5484 (2014).
[65]B. Lu, D. Kang, D. Wang, T. Gao, and J. Dai, "Towards the same line of liquid-liquid phase transition of dense hydrogen from various theoretical predictions," Chin. Phys. Lett. **36**, 103102 (2019).
[66]D. Kang, K. Luo, K. Runge, V. V. Karasiev, and S. B. Trickey, "Two-temperature warm dense hydrogen as a test of quantum protons driven by orbital-free density functional theory electronic forces," Matter Radiat. Extremes (in press) (2020).